iScience

CellPress
OPEN ACCESS

Article

Atypical TGF-β signaling controls neuronal guidance in *Caenorhabditis elegans*

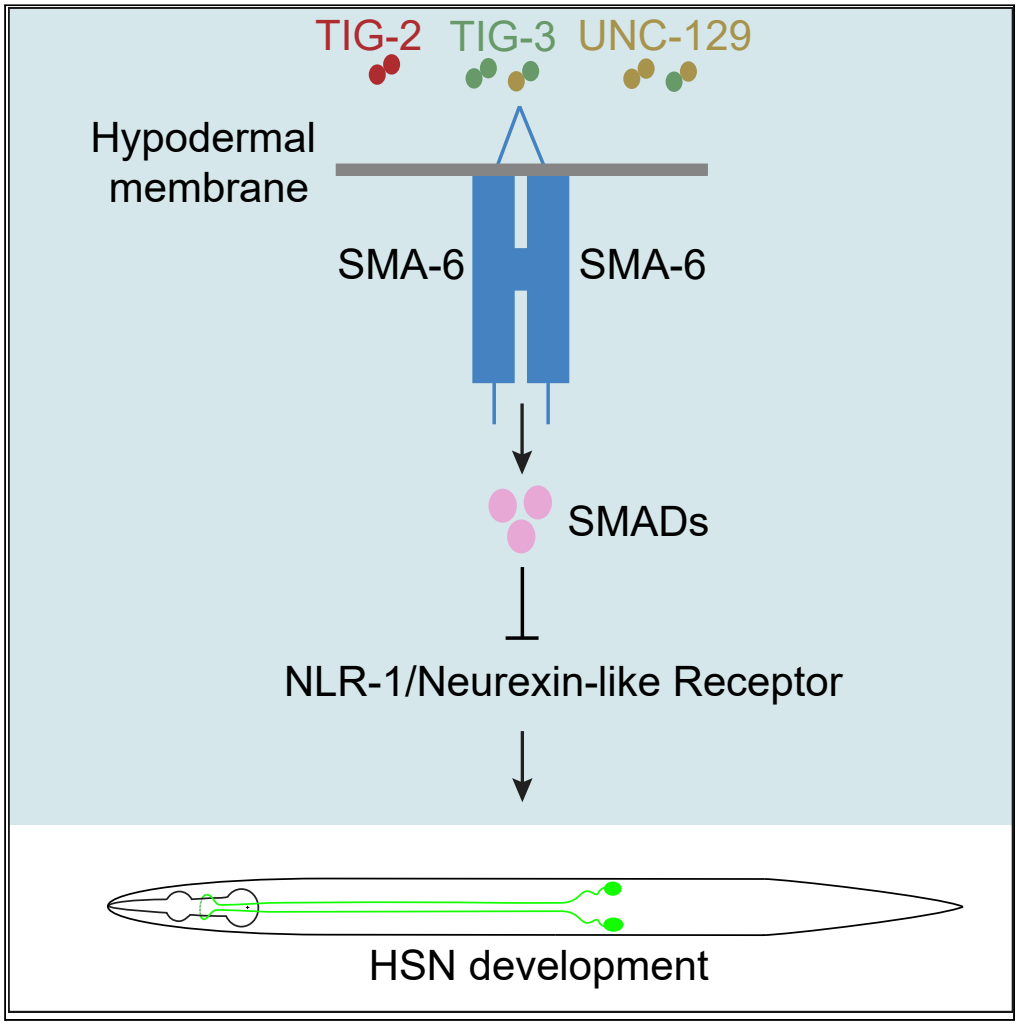

Oguzhan Baltaci, Mikael Egebjerg Pedersen, Tessa Sherry, ..., Matilda Haas, Stuart Archer, Roger Pocock

roger.pocock@monash.edu

Highlights

The *Caenorhabditis elegans* TGF-β type I receptor SMA-6 controls neuronal guidance

SMA-6 acts independently of the TGF-β type II receptor to control neuronal guidance

SMA-6 signaling limits expression of the NLR-1 neurexin-like cell adhesion receptor

Epidermal mis-expression of NLR-1 causes neuronal guidance defects

Baltaci et al., iScience *25*, 103791
February 18, 2022
https://doi.org/10.1016/j.isci.2022.103791

iScience

CellPress
OPEN ACCESS

Article

Atypical TGF-β signaling controls neuronal guidance in *Caenorhabditis elegans*

Oguzhan Baltaci,[1] Mikael Egebjerg Pedersen,[2] Tessa Sherry,[1] Ava Handley,[1] Goda Snieckute,[1,2] Wei Cao,[1] Matilda Haas,[1] Stuart Archer,[3] and Roger Pocock[1,2,4,*]

SUMMARY

Coordinated expression of cell adhesion and signaling molecules is crucial for brain development. Here, we report that the *Caenorhabditis elegans* transforming growth factor β (TGF-β) type I receptor SMA-6 (small-6) acts independently of its cognate TGF-β type II receptor DAF-4 (dauer formation-defective-4) to control neuronal guidance. SMA-6 directs neuronal development from the hypodermis through interactions with three, orphan, TGF-β ligands. Intracellular signaling downstream of SMA-6 limits expression of NLR-1, an essential Neurexin-like cell adhesion receptor, to enable neuronal guidance. Together, our data identify an atypical TGF-β-mediated regulatory mechanism to ensure correct neuronal development.

INTRODUCTION

Brain development requires the generation and assembly of neurons into interconnected circuits. During these highly choreographed processes, neurons are guided by interactions with adjacent cells and the extracellular matrix, which present a variety of cell adhesion and signaling molecules. Among these are the transforming growth factor β (TGF-β) family of cytokines that are critical for metazoan development (Yi et al., 2010). TGF-β ligands control cell signaling by binding to and coordinating cell surface heteromeric type I and type II TGF-β receptor serine/threonine kinases (Shi and Massague, 2003). Upon receptor complex formation, the type II receptor phosphorylates the type I receptor kinase, which transmits the signal by phosphorylating cytoplasmic SMAD (small and mothers against decapentaplegic) proteins (Shi and Massague, 2003). Once phosphorylated, SMAD proteins form complexes that translocate to the nucleus where they interact with nuclear cofactors to regulate target gene transcription (Shi and Massague, 2003). In vertebrates, TGF-β signaling controls multiple aspects of brain development, including neuronal differentiation and migration, axon guidance, and synaptogenesis (Meyers and Kessler, 2017). In addition, the TGF-β family plays extensive roles in neuronal injury and repair (Meyers and Kessler, 2017). However, the role of TGF-β signaling in the *C. elegans* nervous system is not fully understood.

C. elegans encodes a single TGF-β type II receptor (DAF-4) that acts with two TGF-β type I receptors: SMA-6 to control body size/male tail development, and DAF-1 to regulate dauer formation (Figure 1A) (Georgi et al., 1990; Krishna et al., 1999). The TGF-β ligands, DBL-1 and DAF-7, control the SMA-6 and DAF-1 signaling pathways, respectively (Figure 1A) (Golden and Riddle, 1984; Suzuki et al., 1999). However, the function for other putative TGF-β ligands, TIG-2 and TIG-3, are undescribed and UNC-129 controls dorso-ventral axon guidance independently of TGF-β receptors (Figure 1A) (Colavita et al., 1998). Transcriptional output from each *C. elegans* TGF-β pathway is regulated by specific SMAD proteins: SMA-2/3/4 (SMA-6 signaling) and DAF-3/8/14 (DAF-1 signaling) (Savage-Dunn and Padgett, 2017).

In this study, we explored the function of the TGF-β signaling molecules in controlling development of the hermaphrodite-specific neurons (HSNs). Our experiments show that the TGF-β type I receptor SMA-6 acts independently of DAF-4 to control HSN guidance non-cell-autonomously from the hypodermis (epidermis). HSN guidance also requires functional TIG-2, TIG-3, and UNC-129 TGF-β ligands that are released from both the nervous system and muscle. We found that correct SMA-6-directed signaling restricts expression of the NLR-1 Neurexin-like cell adhesion receptor, to enable HSN guidance. Together, our study reveals the ability of a TGF-β type I receptor to control neuronal development independently of a TGF-β type II receptor.

[1]Development and Stem Cells Program, Monash Biomedicine Discovery Institute and Department of Anatomy and Developmental Biology, Monash University, Melbourne, VIC 3800, Australia

[2]Biotech Research and Innovation Centre, University of Copenhagen, Ole Maaløes Vej 5, Copenhagen, Denmark

[3]Monash Bioinformatics Platform, Monash University, Melbourne, VIC 3800, Australia

[4]Lead contact

*Correspondence: roger.pocock@monash.edu

https://doi.org/10.1016/j.isci.2022.103791

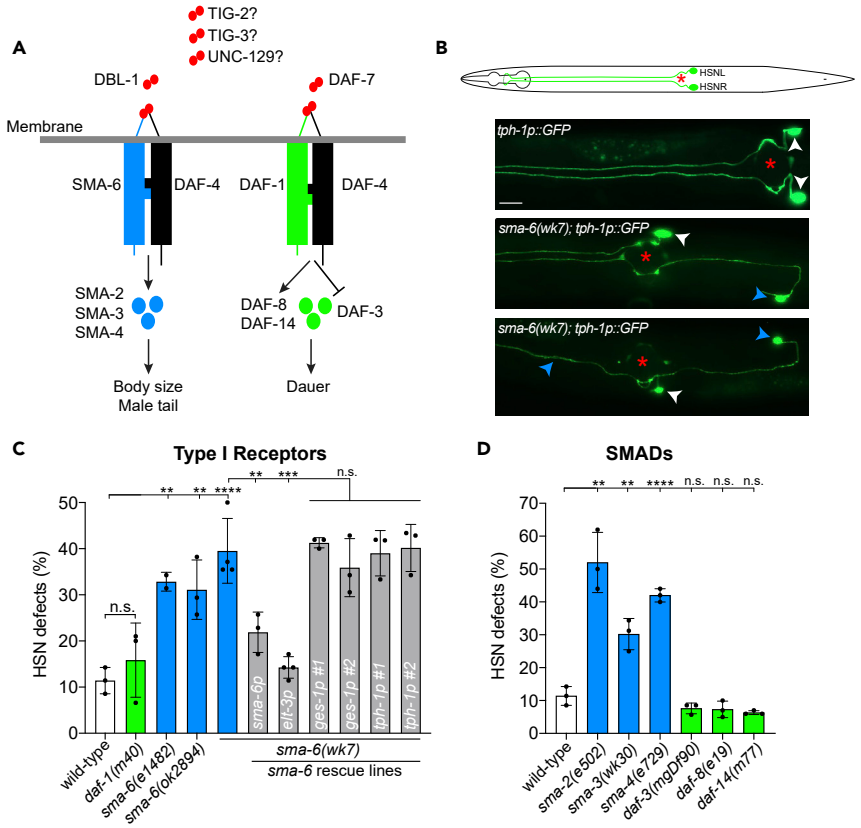

Figure 1. SMA-6, a TGF-β type I receptor controls HSN development

(A) The TGF-β signaling pathways in *C. elegans* control body size/male tail development (left), and dauer formation (right). Each pathway utilizes a common TGF-β type II receptor (DAF-4), and distinct ligands (DBL-1 and DAF-7), TGF-β type I receptors (SMA-6 and DAF-1), and SMAD transcriptional regulators (SMA-2/3/4 and DAF-3/8/14). TIG-2, TIG-3, and UNC-129 are orphan ligands that have not been assigned to either pathway. Receptors are shown as monomers for simplicity.

(B) In wild-type animals (schematic and top panel), HSN cell bodies migrate just posterior to the vulva and extend axons into separate fascicles in the ventral nerve cord. In *sma-6(wk7)* animals, HSN cell bodies under-migrate, and their axons are misguided (middle and bottom panels). Vulval position is marked with a red asterisk, wild-type positioned cell bodies with white arrowheads, and misguided cell bodies and axons with blue arrowheads. HSNs imaged using the *zdIs13(tph-1p::GFP)* transgenic strain. Ventral view, anterior to the left. Scale bar: 20 μm.

(C) Quantification of HSN developmental defects in TGF-β type I receptor mutants *sma-6* and *daf-1*. Loss of *sma-6* but not *daf-1* causes HSN developmental defects. Driving *sma-6* expression using its own promoter or a hypodermal promoter (*elt-3*) rescues *sma-6(wk7)*-induced HSN developmental defects. Driving *sma-6* expression using intestinal (*ges-1*) or HSN (*tph-1*) promoters does not rescue *sma-6(wk7)*-induced HSN developmental defects. # refers to independent transgenic lines. n > 100; **p < 0.01, ***p < 0.001, ****p < 0.0001, n.s. not significant (One-way ANOVA with Tukey's correction). Error bars represent mean ± SEM.

(D) Quantification of HSN developmental defects in animals lacking SMAD transcriptional regulators. Loss of SMADs that control body size and male tail development (SMA-2/3/4) but not dauer SMADs (DAF-3/8/14) causes HSN developmental defects. n > 100; **p < 0.01, ****p < 0.0001, n.s. not significant (One-way ANOVA with Tukey's correction). Error bars represent mean ± SEM.

RESULTS

The TGF-β type I receptor SMA-6 controls neuronal guidance

How TGF-β signaling coordinates gene expression programs to control nervous system development is not fully understood. Here, we used the *C. elegans* HSNs to explore the *in vivo* requirement for TGF-β signaling in neuronal migration and axon guidance. During embryogenesis, the HSNs undergo long-range posterior-anterior migration over hypodermal cells. Later, in juvenile larvae the HSNs extend anteriorly-directed axons over a precisely defined route within the ventral nerve cord before terminating at the nerve ring (Figure 1B) (Desai et al., 1988; Garriga et al., 1993). These developmental events are precisely regulated by

multiple conserved guidance pathways and environmental factors (Adler et al., 2006; Desai et al., 1988; Kinnunen et al., 2005; Pedersen et al., 2013; Pocock and Hobert, 2008). We examined HSN development using a transgenic strain in which the HSN cell bodies and axons are marked with green fluorescent protein (GFP) (Figure 1B). We tested the effect of independently disrupting the two recognized TGF-β pathways in *C. elegans* using mutants for the TGF-β type I receptors SMA-6 (body size/male tail development pathway) and DAF-1 (dauer pathway) (Figures 1A–1C). We found that SMA-6, but not DAF-1, is required for HSN migration and axon guidance (Figures 1B and 1C; Table S1). Analysis of three independently-derived *sma-6* loss-of-function alleles confirmed the importance of SMA-6 for HSN development (Figure 1C). SMA-6 is primarily expressed in the hypodermis, from which it regulates body size, the pharynx and the intestine (Wang et al., 2002; Yoshida et al., 2001). To examine where SMA-6 acts to control HSN development, we restored *sma-6* expression under its own promoter and tissue specific drivers in *sma-6(wk7)* mutant animals (Figure 1C). Expression of *sma-6* cDNA under its own promoter or a hypodermal promoter (*elt-3*) rescued the *sma-6(wk7)* HSN developmental defects (Figure 1C and Table S1) (Gleason et al., 2014). Expression of *sma-6* in the intestine (*ges-1* promoter) or HSNs (*tph-1* promoter) did not rescue HSN developmental defects (Figure 1C and Table S1) (Sze et al., 2000; Zhang and Zhang, 2012). These data show that SMA-6 functions in the hypodermis to non-cell-autonomously control HSN development.

TGF-β type I receptors control the phosphorylation status of downstream SMAD transcriptional regulators. Phosphorylation of SMADs permits their nuclear accumulation where they activate or repress target gene expression. We found that SMADs that act downstream of DAF-1 in the dauer pathway (DAF-3, DAF-8, and DAF-14) are dispensable for HSN development (Figure 1D) (Savage-Dunn and Padgett, 2017). The SMADs acting downstream of SMA-6 to control body size and male tail development are SMA-2, SMA-3, and SMA-4 (Savage-Dunn and Padgett, 2017). We found that loss of *sma-2*, *sma-3* or *sma-4* caused similar penetrance of HSN developmental defects to *sma-6* mutant animals (Figures 1C and 1D; Table S1). We found that loss of SMA-3 did not enhance the *sma-6(ok2894)* mutant phenotype, suggesting they act in the same genetic pathway (Table S1). Further, expression of SMA-3 in the hypodermis (*vha-7* promoter) (Clark et al., 2018) rescued the *sma-3(wk30)* mutant HSN phenotype (Table S1). Together, these data suggest that SMA-6 regulates HSN development from the hypodermis through the canonical transcription factors SMA-2/3/4.

The sole *C. elegans* TGF-β type II receptor DAF-4 is dispensable for neuronal guidance

The SMA-6 TGF-β type I receptor functions in a complex with the sole DAF-4 TGF-β type II receptor to control body size and male tail morphogenesis (Savage-Dunn and Padgett, 2017). Surprisingly, two widely used *daf-4* deletion alleles - *e1364* and *ok828* - exhibited wild-type HSN development (Figures 2A and 2B). These *daf-4* alleles harbor large deletions that lead to premature stop codons, and in the case of *e1364*, elimination of kinase function (Figures 2A and S1) (Gunther et al., 2000). To confirm that DAF-4 is dispensable for HSN development, we generated two additional deletion alleles using CRISPR-Cas9 that introduce frameshifts in exon one of *daf-4* (*rp122* and *rp123*) (Figures 2A and S1) (Dokshin et al., 2018). HSNs developed normally in *rp122* and *rp123* animals, confirming that DAF-4 does not control HSN development (Figure 2B).

Although DAF-4 is dispensable for HSN development, it is conceivable that lack of SMA-6 causes aberrant DAF-4 receptor trafficking or dysregulation of DAF-4-directed signaling. To investigate these possibilities, we first examined the effect of disrupting TGF-β receptor recycling on HSN development. Following endocytosis, TGF-β receptors are trafficked to early endosomes, from where they are either recycled to the plasma membrane for further signaling or conveyed to the lysosome for degradation. A previous study showed that SMA-6 and DAF-4 are recycled through separate mechanisms (Gleason et al., 2014). RME-1 (Eps15 homology-domain containing/receptor mediated endocytosis-1) is a conserved protein required for trafficking of SMA-6 and DAF-4 (Gleason et al., 2014). Loss of *rme-1* reduces SMA-6 levels because of inappropriate lysosomal degradation and causes accumulation of DAF-4 in intracellular vesicles (Gleason et al., 2014). In contrast, ARF-6 (ADP-ribosylation factor-6) specifically controls DAF-4 recycling, where DAF-4 incorrectly accumulates in endosomes of *arf-6* mutants (Gleason et al., 2014). We found that *rme-1(b1045)* mutants exhibit ~30% penetrant HSN defects, like that caused by loss of SMA-6 (Figure 2C). In addition, loss of *rme-1* did not enhance *sma-6(wk7)* HSN defects, suggesting they act in the same genetic pathway (Figure 2C). In contrast, *arf-6(tm1447)* mutants exhibited wild-type HSN development (Figure 2C). Next, we examined whether the HSN developmental defects of *sma-6(wk7)* animals are caused by inappropriate DAF-4 signaling. To this end, we introduced mutants for transcriptional regulators acting downstream of DAF-4 in the dauer pathway into the *sma-6(wk7)* background. We found that neither loss of the antagonistic co-SMAD DAF-3 nor the R-SMAD DAF-14

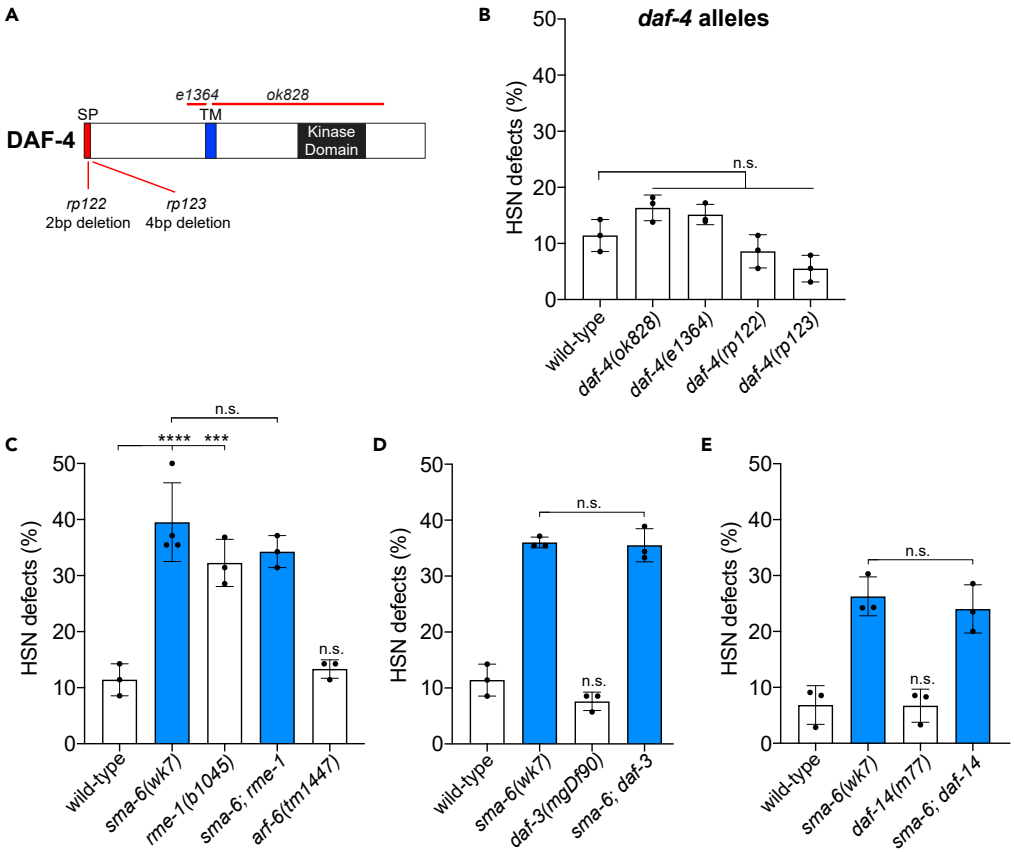

Figure 2. DAF-4, the sole *C. elegans* TGF-β type II receptor, is dispensable for HSN development

(A) Protein domain organization of the DAF-4 TGF-β type II receptor and mutant alleles used in this study. All genetic lesions (red lines) cause frameshifts. SP = signal peptide; TM = transmembrane domain.

(B) Quantification of HSN developmental defects in wild-type and *daf-4* mutant animals. All *daf-4* mutant alleles exhibit wild-type HSN development. n > 100; n.s. not significant (One-way ANOVA with Tukey's correction). Error bars represent mean ± SEM.

(C) Quantification of HSN developmental defects in wild-type, *sma-6(wk7)*, *rme-1(b1045)*, *arf-6(tm1447)*, and *rme-1; sma-6* mutant animals. Loss of retromer-dependent SMA-6 recycling but not ARF-6-dependent DAF-4 recycling causes HSN developmental defects. n > 100; ***p < 0.001, ****p < 0.0001, n.s. not significant (One-way ANOVA with Tukey's correction). Error bars represent mean ± SEM.

(D) Quantification of HSN developmental defects in wild-type, *sma-6(wk7)*, *daf-3(mgDf90)*, and *sma-6; daf-3* mutant animals. n > 100; n.s. not significant (One-way ANOVA with Tukey's correction). Error bars represent mean ± SEM.

(E) Quantification of HSN developmental defects in wild-type, *sma-6(wk7)*, *daf-14(m77)*, and *sma-6; daf-14* mutant animals. n > 100; n.s. not significant (One-way ANOVA with Tukey's correction). Error bars represent mean ± SEM Note: the *mgIs71(tph-1p::GFP)* transgene was used for HSN analysis in (E) which has a lower background HSN phenotype compared to *zdIs13(tph-1p::GFP)*.

agonist altered the *sma-6(wk7)* mutant HSN developmental defects (Figures 2D and 2E). Collectively, our genetic data reveal that the SMA-6 TGF-β type I receptor controls HSN development independently of signaling directed by the TGF-β type II receptor DAF-4.

Three TGF-β ligands interact with SMA-6 to control neuronal guidance

Five putative TGF-β ligands (DAF-7, DBL-1, TIG-2, TIG-3, and UNC-129) are encoded by the *C. elegans* genome, with functions identified for only two of them (DAF-7 and DBL-1) in controlling TGF-β signaling (Golden and Riddle, 1984; Suzuki et al., 1999). We assessed which TGF-β ligand(s) control HSN development. The DAF-7 ligand acts through the DAF-1/DAF-4 receptor complex and was not required for HSN development (Figures 1 and 3A). DBL-1 acts in the body size/male tail development pathway through the SMA-6/DAF-4 receptor complex; however, *dbl-1* was also dispensable for HSN development (Figures 1 and 3A). We next examined the other less studied TGF-β ligands that have not previously been associated, either functionally or physically, with a TGF-

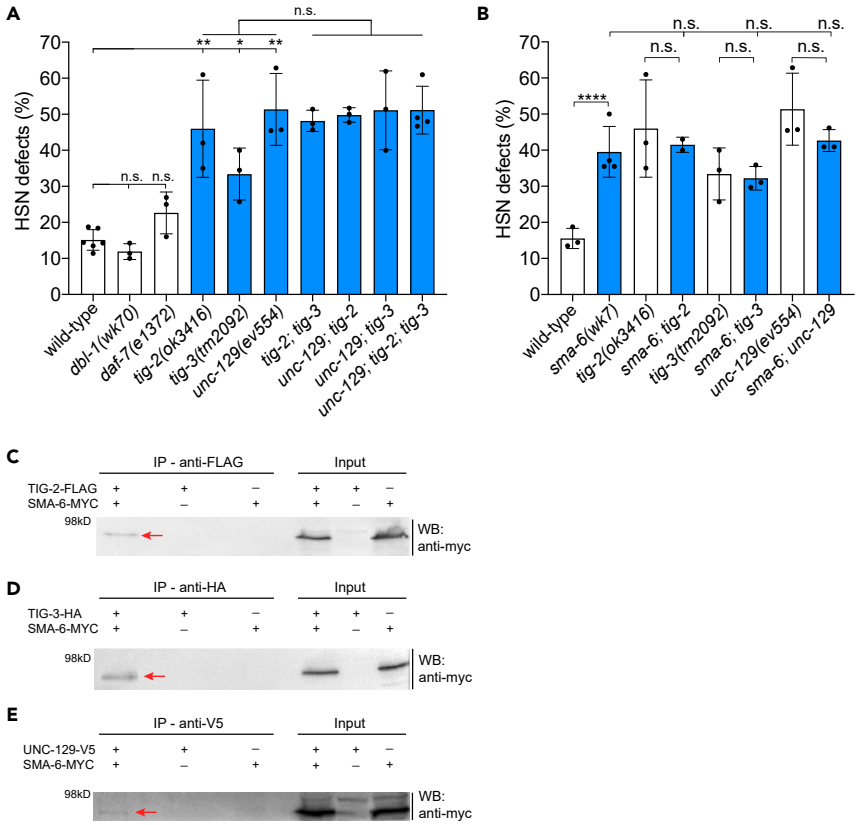

Figure 3. SMA-6 interacts with three, orphan, TGF-β ligands to control HSN development

(A) Quantification of HSN developmental defects in *dbl-1(wk70)*, *daf-7(e1372)*, *tig-2(ok3416)*, *tig-3(tm2092)*, and *unc-129(ev554)* single mutants, and all compound mutant combinations of *tig-2*, *tig-3*, and *unc-129*. *dbl-1* and *daf-7* mutant animals exhibit wild-type HSN development. Loss of either *tig-2*, *tig-3*, or *unc-129* causes HSN developmental defects and the *tig-2; tig-3; unc-129* triple mutant and each double mutant combination is not significantly different from each single mutant. n > 100; *p < 0.05, **p < 0.01, n.s. not significant (One-way ANOVA with Tukey's correction). Error bars represent mean ± SEM.

(B) Quantification of HSN developmental defects in *sma-6(wk7)* animals in combination with either *tig-2(ok3416)*, *tig-3(tm2092)*, or *unc-129(ev554)* mutations. Each double mutant combination is not significantly different from the respective single mutant. n > 100; ****p < 0.0001, n.s. not significant (One-way ANOVA with Tukey's correction). Error bars represent mean ± SEM.

(C–E) Input (total cell lysates) and immunoprecipitates (IP) from transfected HEK293T cells. Proteins detected with antibodies in western blots (WB) as indicated. (C) TIG-2-FLAG co-precipitates with SMA-6-MYC; (D) TIG-3-HA co-precipitates with SMA-6-MYC; (E) UNC-129-V5 co-precipitates with SMA-6-MYC. kD, kilodalton. Immunoprecipitated SMA-6-MYC is marked with a red arrow. Whole blots in Figure S4.

β receptor. Surprisingly, we found that knockout of any one of TIG-2, TIG-3 or UNC-129 caused HSN developmental defects (Figure 3A). Using compound mutant analysis, we examined whether these ligands act in the same genetic pathway to control HSN development. We found that all double mutant combinations and the *tig-2; tig-3; unc-129* triple mutant exhibit the same penetrance and expressivity of HSN developmental defects as the respective single mutants - suggesting they act in concert to control HSN development (Figure 3A and Table S1). UNC-129 was previously shown to control DA/DB axon guidance (Colavita et al., 1998; MacNeil et al., 2009). We examined a potential overlapping role for the TIG-2 and TIG-3 ligands and SMA-6 in DA/DB development but found that UNC-129 acts independently in this context (Figure S2 and Table S1). This supports the presence of context-dependent functions for TGF-β ligands.

tig-2, *tig-3*, and *unc-129* are prominently expressed in body wall muscle (BWM) and the nervous system (Cao et al., 2017). We examined whether the source of these secreted TGF-β ligands is important for HSN development. We performed tissue-specific transgenic rescue experiments by expressing cDNAs of each ligand in BWM or the nervous system in the respective mutant backgrounds (Figure S3) (Fujiwara et al., 1999; Okkema et al.,

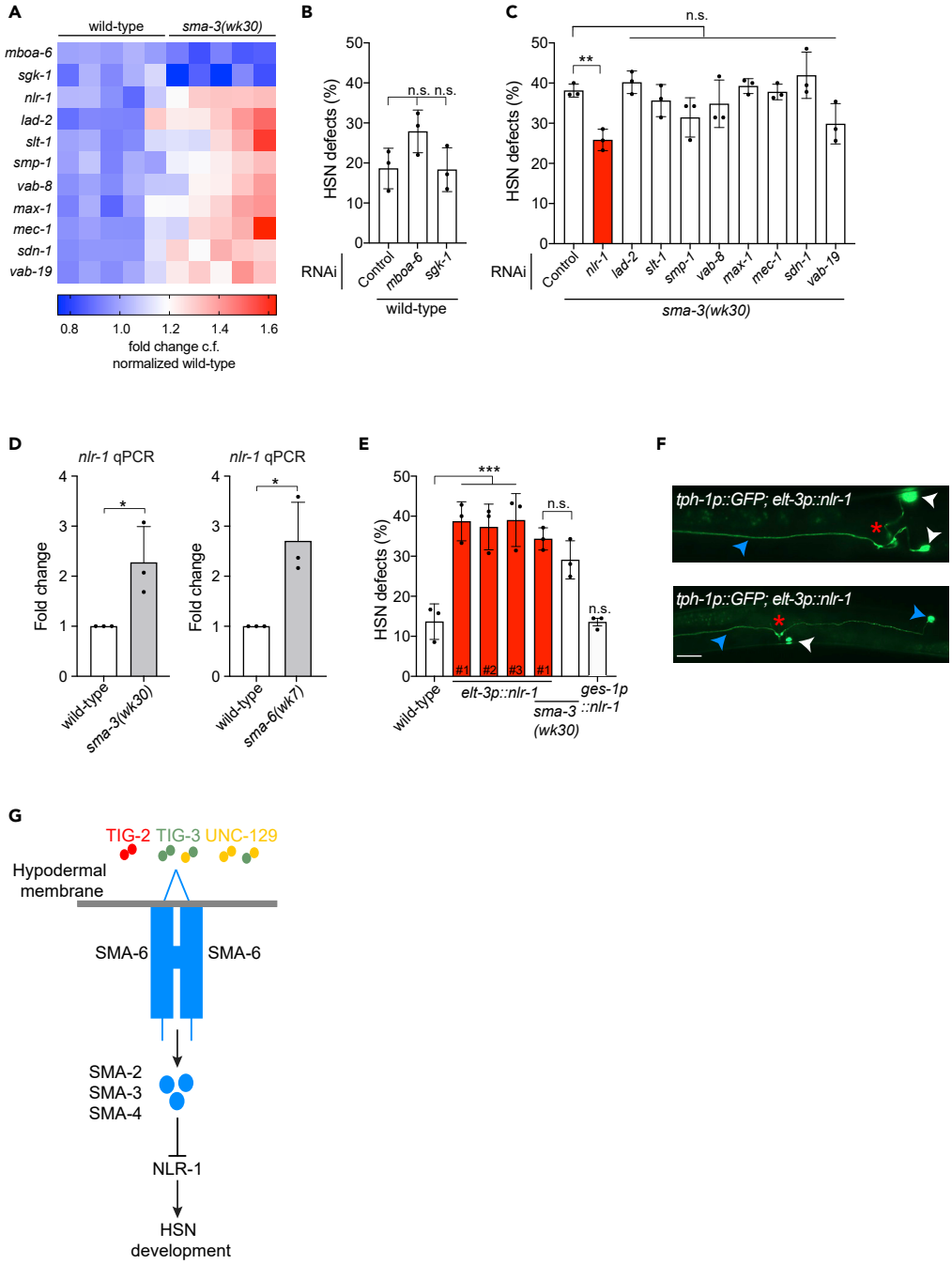

Figure 4. SMA-3 regulation of the NLR-1 Neurexin-like receptor controls HSN development

(A) Heatmap of whole-animal transcriptional profiling from *sma-3(wk30)* L2 larvae compared to wild-type. Gene names of candidate HSN regulators on the left. Each column represents individual total RNA samples. Downregulated (blue), upregulated (red),and unchanged (white).

(B) Quantification of HSN developmental defects in wild-type animals following RNAi knockdown of genes downregulated in the *sma-3(wk30)* mutant. n > 100; n.s. not significant (One-way ANOVA with Tukey's correction). Error bars represent mean ± SEM.

(C) Quantification of HSN developmental defects in *sma-3(wk30)* animals following RNAi knockdown of genes upregulated in the *sma-3(wk30)* mutant. n > 100; **p < 0.01, n.s. not significant (One-way ANOVA with Tukey's correction). Error bars represent mean ± SEM.

Figure 4. *Continued*

(D) Relative *nlr-1* mRNA levels in *sma-3(wk30)* (left) and *sma-6(wk7)* (right) mutant L2 larvae normalized to values for wild-type worms. Three biological replicates were compared (*cdc-42* reference gene was used). *p < 0.05 (t test). Error bars represent mean ± SEM.

(E) Quantification of HSN developmental defects in animals overexpressing *nlr-1* in the hypodermis (*elt-3* promoter) or intestine (*ges-1* promoter). *nlr-1* overexpression in the hypodermis but not the intestine causes HSN defects. HSN defects of *sma-3(wk30)* animals are not enhanced by *nlr-1* overexpression in the hypodermis. n > 100; ***p < 0.001, n.s. not significant (One-way ANOVA with Tukey's correction). Error bars represent mean ± SEM # refers to independent transgenic lines (line #1 in the *sma-3(wk30)* background is the same line used in wild-type).

(F) HSN developmental defects caused by overexpression of *nlr-1* in the hypodermis are phenotypically similar to those observed with loss of *sma-6* and *sma-3* (see Figure 1B and Table S1). Vulval position is marked with a red asterisk; wild-type positioned cell bodies with white arrowheads, and misguided cell bodies and axons with blue arrowheads. Ventral view, anterior to the left. Scale bar: 20 μm.

(G) The TGF-β ligands TIG-2 (red), TIG-3 (green), and UNC-129 (yellow) regulate the TGF-β type I receptor SMA-6 to control HSN guidance non-cell-autonomously from the hypodermis. We hypothesize that TIG-2 homodimers expressed from neurons and TIG-3/UNC-129 homo- or heterodimers expressed from muscle interact with SMA-6. In the hypodermis TGF-β signaling through the SMA-2/3/4 transcriptional regulators limits expression of the Neurexin-like cell adhesion molecule NLR-1 to enable faithful HSN development.

1993). We found that expressing TIG-3 and UNC-129 in BWM rescued HSN developmental defects of the respective mutant (Figure S3). In contrast, TIG-2 expression in the nervous system rescued HSN developmental defects in *tig-2* mutant animals (Figure S3). Further, overexpression of UNC-129 in the nervous system exacerbated HSN developmental defects of the *unc-129* mutant (Figure S3). These data show that correct spatial expression of TGF-β ligands is important for HSN development. We performed further genetic analysis to determine whether *tig-2*, *tig-3,* and *unc-129* act in the same genetic pathway as *sma-6* to control HSN development (Figure 3B and Table S1). We found that the HSN developmental defects of each compound mutant between SMA-6 and the individual ligands was not significantly different from each single mutant (Figure 3B).

Our genetic data suggest that the TIG-2, TIG-3, and UNC-129 ligands control HSN development by interacting with the SMA-6 TGF-β type I receptor. To test this assertion, we investigated whether SMA-6 interacts with TIG-2, TIG-3, and UNC-129 using co-immunoprecipitation (coIP) experiments in human HEK293T cells (Figures 3C–3E). We found that MYC-tagged SMA-6 co-precipitated with TIG-2-FLAG, TIG-3-HA, and UNC-129-V5 (Figures 3C–3E and S4). Together, our genetic and biochemical analysis suggest that the TGF-β ligands TIG-2, TIG-3, and UNC-129 interact with the SMA-6 TGF-β type I receptor and act in the same genetic pathway to control HSN development.

SMA-6 signaling controls neuronal guidance by limiting neurexin expression

How does SMA-6-directed signaling control HSN development? To answer this question, we focused our analysis on SMA-3, an R-SMAD, which controls transcriptional output downstream of SMA-6 signaling and is important for HSN guidance (Figure 1D). We performed RNA sequencing (RNA-seq) to identify differentially expressed genes (DEGs) in *sma-3(wk30)* null mutant animals compared to wild-type at the L2 stage of development, a stage during which the HSN axons extend (Garriga et al., 1993). We identified 406 (FDR <0.05, absolute log2Fc > 0.585) and 2082 (FDR < 0.05) DEGs in *sma-3(wk30)* animals compared to wild-type (Figures 4A, S5, and S6; Tables S2 and S3). Gene ontology (GO) analysis of DEGs revealed enrichment of several biological processes, including those previously associated with the regulation of body size and male tail development (Figure S5) (Huang et al., 2007; Savage-Dunn and Padgett, 2017). However, regulation of neuronal development was not an enriched GO term, suggesting that SMA-3 controls a specific gene to control HSN development. We manually surveyed the DEG lists for molecules with putative or known roles in cell signaling and adhesion - likely architects of HSN development. We identified eleven such DEGs, two downregulated and nine upregulated in *sma-3(wk30)* animals (Figures 4A, S5, and S6; Table S4). To assess functional importance of these DEGs in HSN development, we used RNA-mediated interference (RNAi) (Figures 4A–4C). For the genes downregulated in *sma-3(wk30)* animals, *sgk-1* and *mboa-6,* we knocked down their expression in wild-type animals but no HSN developmental defects were detected (Figure 4B). To assess the potential impact of inappropriate expression of the nine genes upregulated in *sma-3(wk30)* animals, we knocked down their expression in the *sma-3(wk30)* mutant and asked whether HSN developmental defects were suppressed (Figure 4C). We found that RNAi knockdown of *nlr-1* suppressed the HSN defects of *sma-3(wk30)* animals (Figure 4C).

NLR-1 is a member of the Caspr subfamily of neurexin-like proteins (Haklai-Topper et al., 2011). This family of transmembrane cell adhesion molecules mediate neuron-neuron interactions and functionally organize

synapses (Lise and El-Husseini, 2006; Sudhof, 2008). NLR-1 contains extracellular Laminin G, epidermal growth factor, and fibrinogen-related domains, suggesting roles in cell adhesion and cell-cell signaling (Haklai-Topper et al., 2011). A *C. elegans nlr-1* deletion mutant (*tm2050)* causes embryonic lethality (*C. elegans* Gene Knockout Consortium), demonstrating the essential requirement for this protein (C. elegans Deletion Mutant Consortium, 2012). Our RNAi knockdown experiments show that reducing *nlr-1* expression suppresses the HSN defects caused by loss of *sma-3,* suggesting that SMA-6 signaling limits *nlr-1* expression (Figure 4C). We tested this hypothesis by measuring *nlr-1* mRNA abundance in *sma-3(wk30)* and *sma-6(wk7)* mutants compared to wild-type animals. Using qPCR analysis, we found that *nlr-1* expression is increased by approximately 2-fold in the absence of either *sma-3* (as revealed by RNA-seq) or *sma-6* (Figure 3D). These data show that SMA-6 signaling limits *nlr-1* expression.

Because of the hypodermal-specific function of SMA-6 in non-cell-autonomously regulating HSN development (Figure 1C), we predicted that overexpression of *nlr-1* in the hypodermis, and not in another tissue, would cause HSN defects in wild-type animals. We found that *nlr-1* overexpression in the hypodermis (*elt-3* promoter), but not the intestine (*ges-1* promoter), caused HSN defects like those observed in the *sma-3(wk30)* mutant both quantitatively and qualitatively (Figures 4E and 4F; Table S1). Importantly, hypodermal overexpression of *nlr-1* did not further exacerbate *sma-3(wk30)* HSN defects (Figure 4E). These data reveal that SMA-6 signaling in the hypodermis prevents expression of the neurexin-like protein NLR-1 to optimize the extracellular landscape and enable correct HSN development (Figure 4G).

DISCUSSION

We have shown here that the SMA-6 TGF-β type I receptor controls a developmental decision independently of DAF-4 - the sole TGF-β type II receptor in *C. elegans*. To our knowledge, this is the first report of such a function for a TGF-β type I receptor. However, a previous report did reveal that the other *C. elegans* TGF-β type I receptor, DAF-1, acts partially in parallel with DAF-4 to control dauer formation (Gunther et al., 2000). Our data show that SMA-6 acts in the hypodermis to control HSN guidance. DAF-4 is also expressed in this tissue (Gunther et al., 2000), suggesting that SMA-6 regulates HSN guidance from distinct membrane domains or cellular subpopulations within the hypodermis. Intriguingly, we also show that three, orphan, TGF-β ligands (TIG-2, TIG-3, and UNC-129) physically interact with SMA-6, and act in the same genetic pathway with each other and SMA-6 to control HSN development. TIG-2 functions from the nervous system and TIG-3/UNC-129 from BWM in this regard. This posits that TIG-2 homodimers and TIG-3/UNC-129 homodimers or heterodimers form *in vivo* and interact with SMA-6, potentially in a complex with an unidentified receptor(s). A previous study found a similar non-redundant requirement for three Activin ligands (TGF-β superfamily members) in the *Drosophila* retina (Wells et al., 2017). Further, cell-based assays showed that promiscuous interactions between TGF-β superfamily ligands and their receptors enable cells to perceive information encoded by distinct ligand combinations (Antebi et al., 2017). Thus, discrete intracellular responses are dependent on ligand composition and concentration. We found here that the intracellular responses downstream of SMA-6 are coordinated by the SMA-2/3/4 SMAD complex that represses expression of NLR-1, a neurexin-like cell adhesion receptor. Limiting NLR-1 expression is important as its inappropriate expression in the hypodermis causes defective neuronal migration and axon guidance, presumably because of aberrant extracellular adhesion and/or signaling. Together, our results imply that correct brain development requires tight regulation of Neurexin expression to ensure an optimal adhesive and architectural environment for navigating neurons. It will be interesting to determine if TGF-β signaling plays a similar function in vertebrate nervous systems.

Limitations of the study

Although we have shown that SMA-6 can physically interact with the TGF-β ligands (TIG-2, TIG-3, and UNC-129), additional experiments are needed to determine binding specificity, strength, and binding sites between these molecules. In addition, mechanistic understanding of how the three TGF-β ligands act together to control SMA-6 signaling and how SMA-6 controls SMAD activity without the TGF-β type II receptor DAF-4 requires further study. We found that SMA-6 limits expression of the NLR-1 neurexin-like cell adhesion receptor to enable faithful neuronal guidance. How mis-expressed NLR-1 causes neuronal guidance defects is unknown.

STAR★METHODS

Detailed methods are provided in the online version of this paper and include the following:

SUPPLEMENTAL INFORMATION

Supplemental information can be found online at https://doi.org/10.1016/j.isci.2022.103791.

ACKNOWLEDGMENTS

We thank members of Pocock laboratory and Brent Neumann for comments on the manuscript. Some strains used in this study were provided by the *Caenorhabditis* Genetics Center, which is funded by NIH Office of Research Infrastructure Programs (P40 OD010440), and by Shohei Mitani at the National Bioresource Project (Japan). We also thank Rick Padgett for the *elt-3p::sma-6::gfp* plasmid, Jun Liu for the Myc-SMA-6 plasmid, Yuichi Iino for the *rimb-1* promoter, and Yun Zhang for the *sma-6(wk7); ges-1p::sma-6,* and *sma-6(wk7); sma-6p::sma-6* rescue strains. The authors also acknowledge use of the services and facilities of Micromon Genomics at Monash University. Funding: This work was supported by a grant from the European Research Council (ERC Starting Grant number 260807), Monash Biomedicine Discovery Fellowship, NHMRC Project Grant (GNT1105374), NHMRC Senior Research Fellowship (GNT1137645), and a Victorian Endowment for Science, Knowledge and Innovation Fellowship (VIF23) to R.P.

AUTHOR CONTRIBUTIONS

O.B., M.E.P., T.S., A.H., G.S., W.C., M.H., and R.P. performed experiments. S.A. analyzed the RNA sequencing data. R.P. supervised the research and wrote the manuscript.

DECLARATION OF INTERESTS

Authors declare no competing interests.

Received: November 2, 2020
Revised: December 9, 2021
Accepted: January 12, 2022
Published: February 18, 2022

REFERENCES

Adler, C.E., Fetter, R.D., and Bargmann, C.I. (2006). UNC-6/Netrin induces neuronal asymmetry and defines the site of axon formation. Nat. Neurosci. *9*, 511–518.

Antebi, Y.E., Linton, J.M., Klumpe, H., Bintu, B., Gong, M., Su, C., McCardell, R., and Elowitz, M.B. (2017). Combinatorial signal perception in the BMP pathway. Cell *170*, 1184–1196 e1124.

Brenner, S. (1974). The genetics of Caenorhabditis elegans. Genetics *77*, 71–94.

Cao, J., Packer, J.S., Ramani, V., Cusanovich, D.A., Huynh, C., Daza, R., Qiu, X., Lee, C., Furlan, S.N., Steemers, F.J., et al. (2017). Comprehensive single-cell transcriptional profiling of a multicellular organism. Science *357*, 661–667.

Clark, S.G., and Chiu, C. (2003). C. elegans ZAG-1, a Zn-finger-homeodomain protein, regulates axonal development and neuronal differentiation. Development *130*, 3781–3794.

Clark, J.F., Meade, M., Ranepura, G., Hall, D.H., and Savage-Dunn, C. (2018). *Caenorhabditis elegans* DBL-1/BMP regulates lipid accumulation via interaction with insulin signaling. G3 (Bethesda) *8*, 343–351.

Colavita, A., Krishna, S., Zheng, H., Padgett, R.W., and Culotti, J.G. (1998). Pioneer axon guidance by UNC-129, a *C. elegans* TGF-beta. Science *281*, 706–709.

C. elegans Deletion Mutant Consortium (2012). large-scale screening for targeted knockouts in the Caenorhabditis elegans genome. G3 (Bethesda) *2*, 1415–1425.

Colavita, A., Krishna, S., Zheng, H., Padgett, R.W., and Culotti, J.G. (1998). Pioneer axon guidance by UNC-129, a C. elegans TGF-beta. Science *281*, 706–709.

Desai, C., Garriga, G., McIntire, S.L., and Horvitz, H.R. (1988). A genetic pathway for the development of the Caenorhabditis elegans HSN motor neurons. Nature *336*, 638–646.

Dobin, A., Davis, C.A., Schlesinger, F., Drenkow, J., Zaleski, C., Jha, S., Batut, P., Chaisson, M., and Gingeras, T.R. (2013). STAR: ultrafast universal RNA-seq aligner. Bioinformatics *29*, 15–21.

Dokshin, G.A., Ghanta, K.S., Piscopo, K.M., and Mello, C.C. (2018). Robust genome editing with short single-stranded and long, partially single-stranded DNA donors in Caenorhabditis elegans. Genetics *210*, 781–787.

Fraser, A.G., Kamath, R.S., Zipperlen, P., Martinez-Campos, M., Sohrmann, M., and Ahringer, J. (2000). Functional genomic analysis of C. elegans chromosome I by systematic RNA interference. Nature *408*, 325–330.

Fujiwara, M., Ishihara, T., and Katsura, I. (1999). A novel WD40 protein, CHE-2, acts cell-autonomously in the formation of *C. elegans* sensory cilia. Development *126*, 4839–4848.

Garriga, G., Desai, C., and Horvitz, H.R. (1993). Cell interactions control the direction of outgrowth, branching and fasciculation of the HSN axons of *Caenorhabditis elegans*. Development *117*, 1071–1087.

Georgi, L.L., Albert, P.S., and Riddle, D.L. (1990). daf-1, a *C. elegans* gene controlling dauer larva development, encodes a novel receptor protein kinase. Cell *61*, 635–645.

Gleason, R.J., Akintobi, A.M., Grant, B.D., and Padgett, R.W. (2014). BMP signaling requires retromer-dependent recycling of the type I receptor. Proc. Natl. Acad. Sci. U S A *111*, 2578–2583.

Golden, J.W., and Riddle, D.L. (1984). A pheromone-induced developmental switch in *Caenorhabditis elegans*: temperature-sensitive mutants reveal a wild-type temperature-dependent process. Proc. Natl. Acad. Sci. U S A *81*, 819–823.

Gunther, C.V., Georgi, L.L., and Riddle, D.L. (2000). A *Caenorhabditis elegans* type I TGF beta receptor can function in the absence of type II kinase to promote larval development. Development *127*, 3337–3347.

Haklai-Topper, L., Soutschek, J., Sabanay, H., Scheel, J., Hobert, O., and Peles, E. (2011). The neurexin superfamily of *Caenorhabditis elegans*. Gene Expr. Patterns *11*, 144–150.

Huang, D.W., Sherman, B.T., Tan, Q., Collins, J.R., Alvord, W.G., Roayaei, J., Stephens, R., Baseler, M.W., Lane, H.C., and Lempicki, R.A. (2007). The DAVID Gene Functional Classification Tool: a novel biological module-centric algorithm to functionally analyze large gene lists. Genome Biol. *8*, R183.

Kinnunen, T., Huang, Z., Townsend, J., Gatdula, M.M., Brown, J.R., Esko, J.D., and Turnbull, J.E. (2005). Heparan 2-O-sulfotransferase, hst-2, is essential for normal cell migration in *Caenorhabditis elegans*. Proc. Natl. Acad. Sci. U S A *102*, 1507–1512.

Krishna, S., Maduzia, L.L., and Padgett, R.W. (1999). Specificity of TGFbeta signaling is conferred by distinct type I receptors and their associated SMAD proteins in *Caenorhabditis elegans*. Development *126*, 251–260.

Law, C.W., Chen, Y., Shi, W., and Smyth, G.K. (2014). voom: Precision weights unlock linear model analysis tools for RNA-seq read counts. Genome Biol *15*, R29.

Liao, Y., Smyth, G.K., and Shi, W. (2014). featureCounts: an efficient general purpose program for assigning sequence reads to genomic features. Bioinformatics *30*, 923–930.

Lise, M.F., and El-Husseini, A. (2006). The neuroligin and neurexin families: from structure to function at the synapse. Cell. Mol. Life Sci. *63*, 1833–1849.

MacNeil, L.T., Hardy, W.R., Pawson, T., Wrana, J.L., and Culotti, J.G. (2009). UNC-129 regulates the balance between UNC-40 dependent and independent UNC-5 signaling pathways. Nat. Neurosci. *12*, 150–155.

Mello, C.C., Kramer, J.M., Stinchcomb, D., and Ambros, V. (1991). Efficient gene transfer in *C.elegans*: extrachromosomal maintenance and integration of transforming sequences. Embo J. *10*, 3959–3970.

Meyers, E.A., and Kessler, J.A. (2017). TGF-beta family signaling in neural and neuronal differentiation, development, and function. Cold Spring Harb. Perspect. Biol. *9*, a022244.

Okkema, P.G., Harrison, S.W., Plunger, V., Aryana, A., and Fire, A. (1993). Sequence requirements for myosin gene expression and regulation in Caenorhabditis elegans. Genetics *135*, 385–404.

Pedersen, M.E., Snieckute, G., Kagias, K., Nehammer, C., Multhaupt, H.A., Couchman, J.R., and Pocock, R. (2013). An epidermal microRNA regulates neuronal migration through control of the cellular glycosylation state. Science *341*, 1404–1408.

Pocock, R., and Hobert, O. (2008). Oxygen levels affect axon guidance and neuronal migration in Caenorhabditis elegans. Nat. Neurosci. *11*, 894–900.

Savage-Dunn, C., and Padgett, R.W. (2017). The TGF-beta family in *Caenorhabditis elegans*. Cold Spring Harb. Perspect. Biol. *9*, a022178.

Shi, Y., and Massague, J. (2003). Mechanisms of TGF-beta signaling from cell membrane to the nucleus. Cell *113*, 685–700.

Sudhof, T.C. (2008). Neuroligins and neurexins link synaptic function to cognitive disease. Nature *455*, 903–911.

Suzuki, Y., Yandell, M.D., Roy, P.J., Krishna, S., Savage-Dunn, C., Ross, R.M., Padgett, R.W., and Wood, W.B. (1999). A BMP homolog acts as a dose-dependent regulator of body size and male tail patterning in *Caenorhabditis elegans*. Development *126*, 241–250.

Sze, J.Y., Victor, M., Loer, C., Shi, Y., and Ruvkun, G. (2000). Food and metabolic signalling defects in a Caenorhabditis elegans serotonin-synthesis mutant. Nature *403*, 560–564.

Tian, C., Shi, H., Xiong, S., Hu, F., Xiong, W.C., and Liu, J. (2013). The neogenin/DCC homolog UNC-40 promotes BMP signaling via the RGM protein DRAG-1 in C. elegans. Development *140*, 4070–4080.

Tomioka, M., Naito, Y., Kuroyanagi, H., and Iino, Y. (2016). Splicing factors control C. elegans behavioural learning in a single neuron by producing DAF-2c receptor. Nat Commun *7*, 11645.

Wang, J., Tokarz, R., and Savage-Dunn, C. (2002). The expression of TGFbeta signal transducers in the hypodermis regulates body size in *C. elegans*. Development *129*, 4989–4998.

Wells, B.S., Pistillo, D., Barnhart, E., and Desplan, C. (2017). Parallel Activin and BMP signaling coordinates R7/R8 photoreceptor subtype pairing in the stochastic *Drosophila* retina. Elife *6*, e25301.

Yi, J.J., Barnes, A.P., Hand, R., Polleux, F., and Ehlers, M.D. (2010). TGF-beta signaling specifies axons during brain development. Cell *142*, 144–157.

Yoshida, S., Morita, K., Mochii, M., and Ueno, N. (2001). Hypodermal expression of *Caenorhabditis elegans* TGF-beta type I receptor SMA-6 is essential for the growth and maintenance of body length. Dev. Biol. *240*, 32–45.

Zhang, X., and Zhang, Y. (2012). DBL-1, a TGF-beta, is essential for *Caenorhabditis elegans* aversive olfactory learning. Proc. Natl. Acad. Sci. U S A *109*, 17081–17086.

STAR★METHODS

KEY RESOURCES TABLE

REAGENT or RESOURCE	SOURCE	IDENTIFIER
Antibodies		
Goat anti-Rabbit IgG (H+L) secondary antibody, HRP conjugate	Thermo Fisher Scientific	65-6120
Goat anti-Mouse IgG (H+L) secondary antibody, HRP conjugate	Thermo Fisher Scientific	32430
Mouse anti-FLAG/DYKDDDDK tag antibody	Cell Signaling	2368
Mouse anti-Histidine tag antibody	Bio-Rad	AD1.1.10
Mouse anti-V5 tag antibody	Bio-Rad	SV5-Pk1
Rabbit anti-Myc tag antibody	Abcam	ab9106
Bacterial and virus strains		
Bacteria *Escherichia coli* HT115	CAENORHABDITIS GENETICS CENTER (CGC)	N/A
Bacteria *Escherichia coli* OP50	CAENORHABDITIS GENETICS CENTER (CGC)	N/A
Chemicals, peptides, and recombinant proteins		
cOmplete™, EDTA-free Protease Inhibitor Cocktail	Merck	11836170001
Dynabeads Protein G	Thermo Fisher Scientific	1003D
Lipofectamine 2000 transfection reagent	Thermo Fischer Scientific	11668027
Sodium azide	Sigma	S8032-25G
Critical commercial assays		
Fast SYBR™ Green Master Mix	Thermo Fisher Scientific	4385610
ImProm-II™ Reverse Transcription System	Promega	A3800
In-Fusion® HD Cloning Kit	Takara Bio	102518
Qubit DNA HS kit	Thermo Fisher Scientific	Q33230
RNAeasy mini kit	Qiagen	74104
The LightCycler® 480 SYBR Green I Master	Roche	4707516001
TruSeq Stranded mRNA Sample Prep Kit	Illumina	20020594
Deposited data		
RNA-seq data deposited into NCBI Gene Expression Omnibus	This paper	GEO: GSE63473
Experimental models: Cell lines		
HEK293T	N/A	N/A
Experimental models: Organisms/strains		
C. elegans: Strain RJP18: *rpEx6[tph-1p::gfp]*	This study	RJP18
C. elegans: Strain *RJP1153*: *daf-7(e1372); zdIs13[tph-1p::GFP]*	This study	RJP1153
C. elegans: Strain RJP1154: *daf-1(m40); zdIs13[tph-1p::GFP]*	This study	RJP1154
C. elegans: Strain RJP1330: *tig-2(ok3416); zdIs13[tph-1p::GFP]*	This study	RJP1330
C. elegans: Strain RJP1334: *tig-3(tm2092); zdIs13[tph-1p::GFP]*	This study	RJP1334

(*Continued on next page*)

Continued

REAGENT or RESOURCE	SOURCE	IDENTIFIER
C. elegans: Strain RJP1398: *sma-4(e729); zdIs13[tph-1p::GFP]*	This study	RJP1398
C. elegans: Strain RJP1551: *sma-6(wk7); zdIs13[tph-1p::GFP]*	This study	RJP1551
C. elegans: Strain RJP1553: *sma-6(wk7); zdIs13[tph-1p::GFP]; yxEx615[sma-6p::sma-6; unc-122:GFP]*	This study	RJP1553
C. elegans: Strain RJP1554: *sma-2(e502); zdIs13[tph-1p::GFP]*	This study	RJP1554
C. elegans: Strain RJP1555: *daf-14(m77); mgIs71[tph-1p::GFP]*	This study	RJP1555
C. elegans: Strain RJP1611: *daf-8(e1393); zdIs13[tph-1p::GFP]*	This study	RJP1611
C. elegans: Strain RJP1917: *tig-2(ok3416); tig-3(tm2092); zdIs13[tph-1p::GFP]*	This study	RJP1917
C. elegans: Strain RJP2018: *sma-6(e1482); zdIs13[tph-1p::GFP]*	This study	RJP2018
C. elegans: Strain RJP3203: *mgIs71[tph-1p::GFP]* (original strain GR1333 - backcrossed to N2)	Sze et al., 2000	RJP3203
C. elegans: Strain RJP3333: *sma-3(wk30); zdIs13[tph-1p::GFP]*	This study	RJP3333
C. elegans: Strain RJP3393: *zdIs13[tph-1p::GFP]* (original strain SK4013 - backcrossed to N2)	Clark and Chiu., 2003	RJP3393
C. elegans: Strain RJP3519: *daf-4(e1364); zdIs13[tph-1p::GFP]*	This study	RJP3519
C. elegans: Strain RJP3520: *daf-4(ok828); zdIs13[tph-1p::GFP]*	This study	RJP3520
C. elegans: Strain RJP3603: *sma-6(wk7); tig-2(ok3416); zdIs13[tph-1p::GFP]*	This study	RJP3603
C. elegans: Strain RJP3755: *sma-6(ok2894); zdIs13[tph-1p::GFP]*	This study	RJP3755
C. elegans: Strain RJP3786: *dbl-1(wk70); zdIs13[tph-1p::GFP]*	This study	RJP3786
C. elegans: Strain RJP3800: sma-6(wk7); rme-1(b1045); zdIs13[tph-1p::GFP]	This study	RJP3800
C. elegans: Strain RJP3821: unc-129(ev554); rpEx6[tph-1p::gfp]	This study	RJP3821
C. elegans: Strain RJP3837: *sma-6(wk7); tig-3(tm2092); zdIs13[tph-1p::GFP]*	This study	RJP3837
C. elegans: Strain RJP3843: *rme-1(b1045); zdIs13[tph-1p::GFP]*	This study	RJP3843
C. elegans: Strain RJP3871: *arf-6(tm1447); mgIs71[tph-1p::GFP]*	This study	RJP3871
C. elegans: Strain RJP4047: *daf-4(rp122); zdIs13[tph-1p::GFP]*	This study	RJP4047
C. elegans: Strain RJP4048: *daf-4(rp123); zdIs13[tph-1p::GFP]*	This study	RJP4048
C. elegans: Strain RJP4070: *sma-6(wk7); unc-129(ev554); rpEx6[tph-1p::GFP]*	This study	RJP4070

(*Continued on next page*)

Continued

REAGENT or RESOURCE	SOURCE	IDENTIFIER
C. elegans: Strain RJP4158: *sma-6(wk7); zdIs13[tph-1p::GFP]; yxEx765[ges-1p::sma-6; unc-122p::GFP]*	This study	RJP4158
C. elegans: Strain RJP4161: *unc-129(ev554); tig-2(ok3416); rpEx6[tph-1p::GFP]*	This study	RJP4161
C. elegans: Strain RJP4162: *unc-129(ev554); tig-3(tm2092); rpEx6[tph-1p::GFP]*	This study	RJP4162
C. elegans: Strain RJP4163: *unc-129(ev554); tig-2(ok3416); tig-3(tm2092); rpEx6[tph-1p::GFP]*	This study	RJP4163
C. elegans: Strain RJP4167: *daf-3(mgDf90); zdIs13[tph-1p::GFP]*	This study	RJP4167
C. elegans: Strain RJP4217: *sma-6(wk7); zdIs13[tph-1p::GFP]; rpEx1792[tph-1p:: sma-6 + myo-2p::mCherry]*	This study	RJP4217
C. elegans: Strain RJP4218: *sma-6(wk7); zdIs13[tph-1p::GFP]; rpEx1793[tph-1p:: sma-6 + myo-2p::mCherry]*	This study	RJP4218
C. elegans: Strain RJP4446: *sma-6(wk7); zdIs13[tph-1p::GFP]; rpEx1904[elt-3p:: sma-6::GFP + myo-2p::mCherry]*	This study	RJP4446
C. elegans: Strain RJP4509: *sma-6(wk7); daf-3(mgDf90); zdIs13[tph-1p::GFP]*	This study	RJP4509
C. elegans: Strain RJP4570: *zdIs13 [tph-1p::GFP]; rpEx2034[elt-3p::nlr-1 cDNA + myo-2p::mCherry]*	This study	RJP4570
C. elegans: Strain RJP4571: *zdIs13 [tph-1p::GFP]; rpEx2035[elt-3p::nlr-1 cDNA + myo-2p::mCherry]*	This study	RJP4571
C. elegans: Strain RJP4572: *zdIs13[tph-1p::GFP]; rpEx2036[elt-3p::nlr-1 cDNA+ myo-2p::mCherry]*	This study	RJP4572
C. elegans: Strain RJP4655: *tig-2(ok3416); zdIs13[tph-1p::GFP]; rpEx2079[rimb-1p:: tig-2 cDNA + myo-2p::mCherry]*	This study	RJP4655
C. elegans: Strain RJP4657: *tig-2(ok3416); zdIs13[tph-1p::GFP]; rpEx2081[myo-3p:: tig-2 cDNA + myo-2p::mCherry]*	This study	RJP4657
C. elegans: Strain RJP4660: *tig-3(tm2092); zdIs13[tph-1p::GFP]; rpEx2084[rimb-1p:: tig-3 cDNA + myo-2p::mCherry]*	This study	RJP4660
C. elegans: Strain RJP4663: *tig-3(tm2092); zdIs13[tph-1p::GFP]; rpEx2087[myo-3p:: tig-3 cDNA + myo-2p::mCherry]*	This study	RJP4663
C. elegans: Strain RJP4666: *unc-129(ev554); rpEx6[tph-1p::gfp]; rpEx2090[rimb-1p:: unc-129 cDNA + myo-2p::mCherry]*	This study	RJP4666
C. elegans: Strain RJP4669: *unc-129(ev554); rpEx6[tph-1p::gfp]; rpEx2093[myo-3p::unc-129 cDNA + myo-2p::mCherry]*	This study	RJP4669
C. elegans: Strain RJP4672: *zdIs13[tph-1p::GFP]; rpEx2096[ges-1p::nlr-1 cDNA + myo-2p::mCherry]*	This study	RJP4672

(*Continued on next page*)

Continued

REAGENT or RESOURCE	SOURCE	IDENTIFIER
C. elegans: Strain RJP4675: *sma-3(wk30); zdIs13[tph-1p::GFP]; rpEx2035[elt-3p::nlr-1 cDNA+ myo-2p::mCherry]*	This study	RJP4675
C. elegans: Strain RJP4753: *evIs82b[unc-129:: GFP + dpy-20(+)]*	Colavita and Culotto., 1998	RJP4753
C. elegans: Strain RJP4825: *sma-6(wk7); daf-14(m77); mgIs71[tph-1p::GFP]*	This study	RJP4825
C. elegans: Strain RJP5147: *sma-6(ok2894); sma-3(wk30); zdIs13[tph-1p::GFP]*	This study	RJP5147
C. elegans: Strain RJP5175: *sma-3(wk30); zdIs13[tph-1p::GFP]; qcIs55[vha-7p::gfp:: sma-3 + rol-6]*	This study	RJP5175
C. elegans: Strain RJP5176: *unc-129(ev554) evIs82b*	This study	RJP5176
C. elegans: Strain RJP5177: *sma-6(wk7); evIs82b*	This study	RJP5177
C. elegans: Strain RJP5178: *tig-2(ok3416); evIs82b*	This study	RJP5178
C. elegans: Strain RJP5179: *tig-3(tm2092); evIs82b*	This study	RJP5179
C. elegans: Strain RJP5180: *tig-2(ok3416); tig-3(tm2092); evIs82b*	This study	RJP5180
C. elegans: Strain RJP5181: *tig-2(ok3416); unc-129(ev554) evIs82b*	This study	RJP5181
C. elegans: Strain RJP5182: *tig-3(tm2092); unc-129(ev554) evIs82b*	This study	RJP5182
C. elegans: Strain RJP5183: *tig-2(ok3416); tig-3(tm2092); unc-129(ev554) evIs82b*	This study	RJP5183
C. elegans: Strain ZC1334: *sma-6(wk7); yxEx615[sma-6p::sma-6; unc-122p::gfp]*	Zhang and Zhang, 2012	ZC1334
C. elegans: Strain ZC1573: *sma-6(wk7); yxEx765[ges-1p::sma-6; unc-122p::gfp]*	Zhang and Zhang, 2012	ZC1573
Oligonucleotides		
Genotyping and cloning oligos available on request		
Recombinant DNA		
Plasmid: pRG62 *elt-3p::sma-6::GFP*	Rick Padgett	Gleason et al., 2014
Plasmid: *tph-1p::sma-6::GFP*	This study	
Plasmid: *elt-3p::nlr-1* cDNA	This study	
Plasmid: *ges-1p::nlr-1 cDNA*	This study	
Plasmid: *myo-3p::tig-2 cDNA*	This study	
Plasmid: *myo-3p::tig-3 cDNA*	This study	
Plasmid: *myo-3p::unc-129 cDNA*	This study	
Plasmid: *rimb-1p::tig-2 cDNA*	This study	Tomioka et al., 2016 (*rimb-1* promoter)
Plasmid: *rimb-1p::tig-3 cDNA*	This study	Tomioka et al., 2016 (*rimb-1* promoter)
Plasmid: *rimb-1p::unc-129 cDNA*	This study	Tomioka et al., 2016 (*rimb-1* promoter)
Plasmid: pJKL964 Myc-sma-6	Jun Liu	Tian et al., 2013
Plasmid: pcDNA 3.1 (zeo) tig-2-FLAG	This study	
Plasmid: pcDNA 3.1 (zeo) tig-3-HA	This study	
Plasmid: pcDNA 3.2 unc-129-V5	This study	
Software and algorithms		
Prism	GraphPad	https://www.graphpad.com

RESOURCE AVAILABILITY

Lead contact

- Further information and requests for resources and reagents should be directed to and will be fulfilled by the lead contact, Roger Pocock (roger.pocock@monash.edu).

Materials availability

- Plasmids and *Caenorhabditis elegans* strains generated in this study are available from the lead contact on request.

Data and code availability

- RNA-seq data has been deposited into the NCBI Gene Expression Omnibus (GEO) under accession number GSE151035.
- This paper does not report original code.
- Any additional information required to reanalyse the data reported in this paper is available from the lead contact upon request.

EXPERIMENTAL MODEL AND SUBJECT DETAILS

Nematode strains and genetics

C. elegans strains were grown using standard conditions on NGM agar at 20°C on *Escherichia coli* OP50, unless otherwise stated (Brenner, 1974). All strains were backcrossed to wild-type (N2 Bristol) at least three times prior to scoring. *mgIs71 Is[tph-1p::gfp], zdIs13 Is[tph-1p::gfp]* or *rpEx6[tph-1p::gfp]* were used to score HSN anatomy and *evIs82b Is[unc-129p::gfp)* was used to score DA/DB axon guidance. Detailed strain information can be found in Key Resources Table.

Cell culture

For *in vitro* studies, Human embryonic kidney (HEK293T) cells were cultured using DMEM with 10% FBS and 5 μM L-glutamine at 37°C. Cells were transfected using Lipofectamine 2000 reagent (Invitrogen) according to the manufacturer's protocol.

METHOD DETAILS

Microinjection and transgenic animal generation

Rescue and overexpression plasmids were delivered into wild-type or mutant hermaphrodites at 1–10 ng/μl concentration by microinjection (Mello et al., 1991). *myo-2p::mCherry* (5 ng/μl) was used as an injection marker.

Fluorescence microscopy

Animals were mounted on 5% agar pads, anesthetized with 20 μM sodium azide and examined using an automated fluorescence microscope (Zeiss, AXIO Imager M2) and ZEN software (version 3.1).

C. elegans plasmid generation

tph-1p::sma-6 rescue plasmid. *tph-1p::sma-6* was generated by cloning the 2650 bp full-length *sma-6* genomic sequence into the pPD49.26 plasmid (containing a 1748 bp *tph-1* promoter) using *NheI*.

myo-3p::tig-2 cDNA rescue plasmid. *myo-3p::tig-2* was generated by cloning the 1101 bp full-length *tig-2* cDNA into the pPD95.86 plasmid (containing a 2385 bp *myo-3* promoter) using *NheI-KpnI*.

myo-3p::tig-3 cDNA rescue plasmid. *myo-3p::tig-3* was generated by cloning the 756 bp full-length *unc-129* cDNA into the pPD95.86 plasmid (containing a 2385 bp *myo-3* promoter) using *NheI-KpnI*.

myo-3p::unc-129 cDNA rescue plasmid. *myo-3p::unc-129* was generated by cloning the 1224 bp full-length *tig-3* cDNA into the pPD95.86 plasmid (containing a 2385 bp *myo-3* promoter) using *NheI-KpnI*.

rimb-1p::tig-2 cDNA rescue plasmid. *rimb-1p::tig-2* was generated by cloning the 1101 bp full-length *tig-2* cDNA into the *rimb-1p::daf-2a* (containing a 2479 bp *rimb-1* promoter) using PCR fusion to replace the *daf-2a* coding sequence.

rimb-1p::tig-3 cDNA rescue plasmid. *rimb-1p::tig-3* was generated by cloning the 756 bp full-length *tig-3* cDNA into the *rimb-1p::daf-2a* (containing a 2479 bp *rimb-1* promoter) using PCR fusion to replace the *daf-2a* coding sequence.

rimb-1p::unc-129 cDNA rescue plasmid. *rimb-1p::unc-129* was generated by cloning the 1224 bp full-length *unc-129* cDNA into the *rimb-1p::daf-2a* (containing a 2479 bp *rimb-1* promoter) using PCR fusion to replace the *daf-2a* coding sequence.

elt-3p::nlr-1 cDNA overexpression plasmid. *elt-3p::nlr-1* was generated by cloning the 3543 bp full-length *nlr-1* cDNA into the pPD49.26 plasmid using *NcoI*. The 2057 bp *elt-3* promoter was then cloned into this plasmid using PCR fusion.

ges-1p::nlr-1 cDNA overexpression plasmid. *ges-1p::nlr-1* was generated by cloning the 3543 bp full-length *nlr-1* cDNA into the pPD49.26-*ges-1p* plasmid using *NheI-NcoI*. This plasmid includes the 3272 bp *ges-1* promoter.

tig-2-FLAG mammalian expression plasmid. *tig-2-FLAG* (C-terminal tag) was generated by cloning the 1098 bp full-length *tig-2* cDNA without the stop codon into the pcDNA3.1(zeo) mammalian expression plasmid using *NheI-HindIII*.

tig-3-HA mammalian expression plasmid. *tig-3-HA* (C-terminal tag) was generated by cloning the 753 bp full-length *tig-3* cDNA without the stop codon into the pcDNA3.1(zeo) mammalian expression plasmid using *NheI-KpnI*.

unc-129-V5 mammalian expression plasmid. *unc-129-V5* (C-terminal tag) was generated by cloning the 1224 bp full-length *unc-129* cDNA without the stop codon into the Wnt3A-V5 mammalian expression plasmid (Addgene, plasmid #43810) using PCR fusion to replace the Wnt3A coding sequence.

CRISPR-Cas9

daf-4 mutant alleles. Two single guide RNAs (sgRNA) targeting the first exon of *daf-4* were designed using a CRISPR design tool (http://crispr.mit.edu). The sgRNAs (GCCCATTTCCTATAAGGTGC and CTAC AAGAACCTTACAAGAG) were independently cloned into the Cas9 plasmid using In-Fusion® HD Cloning Kit (Takara Bio, USA) and confirmed by Sanger sequencing. Plasmids were injected into wild-type hermaphrodites at a final concentration of 50 ng/μl per plasmid. The *daf-4* CRISPR-knockout candidates were individually selected on Sma and/or dauer phenotype, and incubated at 15°C to enable dauer recovery. CRISPR-Cas9-induced mutations were identified by Sanger sequencing using PCR products amplified from the *daf-4* gene. Two independent alleles were identified, *rp122* and *rp123*, which possess frameshift mutations resulting with premature stop codons. These mutant strains were backcrossed to wild-type males three times prior to analysis.

RNAi experiments

RNAi feeding experiments were conducted following the Ahringer lab protocol (Fraser et al., 2000). L4440 plasmids (with or without specific dsRNA) were transformed in *Escherichia coli* HT115 and selected with ampicillin and tetracycline. Four L4 hermaphrodites were moved into each RNAi bacteria seeded plate and progeny were scored after 4 days as young adults. For each knockdown strain, three different experiments were conducted on three independent days.

Co-immunoprecipitation and western blotting

Immunoprecipitation was performed using Dynabeads™ Protein G (10003D, Thermo Fisher Scientific). Briefly, cells were cultured in 6-well plates for one day to 70% confluency and transfected with *tig-2-FLAG*, *tig-3-HA* and *unc-129-V5* individually and in combination with *sma-6-Myc* to test the interactions. Cells were lysed with lysis buffer (Tris, NaCl, SDS, Triton X-100) after 24 hours of incubation. Lysates

were incubated with Dynabeads™ Protein and specific primary antibodies (see antibodies section). Immunoprecipitates were washed 3 times using lysis buffer and proteins were eluted with 2.5X LDS buffer. Proteins were separated on 12.5% sodium dodecyl sulfate polyacrylamide gels and screened by western blot using the appropriate primary and secondary antibodies.

Antibodies

The primary antibodies used in this study were rabbit anti-myc (ab9106, abcam), mouse anti-flag (2368, Cell Signaling), mouse anti-V5 (SV5-Pk1, Bio-Rad) and rabbit anti-HA (C29F4, Cell signaling). The secondary antibodies used in this study were goat anti-rabbit IgG (H+L), HRP conjugate (65-6120, Life Technologies) and goat anti-mouse IgG (H+L), HRP conjugate (32430, Life Technologies).

RNA extraction

Approximately 2000 non-starved, synchronized L2-stage animals were washed three times in M9 buffer and pelleted. 100 µl of M9 and 500µl Trizol (Agilent) was added to each worm pellet and frozen at −80°C. Samples were freeze-thawed in liquid nitrogen and 37°C, a total of 7 times. The RNA was chloroform-extracted and purified using the RNeasy Mini Kit (Qiagen), according to manufacturer's protocol.

RNA sequencing

RNA sequencing was performed at Micromon Genomics (Monash University). mRNA samples were converted to indexed Illumina sequencing libraries using Illumina's TruSeq Stranded mRNA Sample Prep Kit, employing oligo (dT)-conjugated beads to enrich for polyadenylated transcripts. Libraries were quantitated using a Qubit DNA HS kit (Invitrogen, Carlsbad CA., USA), sized using an AATI Fragment Analyzer (Advanced Analytical Technologies Inc., USA), and sequenced on an Illumina NextSeq500 configured to produce 75 nt paired-end reads. Fastq files were generated by bcl2fastq, trimming 3' adapter sequences.

Bioinformatics for RNA sequencing

RNA-seq data was converted to a per-gene read-count matrix using RNAsik pipeline v1.5.0. Briefly, single-end reads were mapped to the *C. elegans* genome (WBcel235) using STAR (Dobin et al., 2013) in splice-aware mode, duplicates were marked using Picard Markduplicates, and reads were assigned to gene models (exonic only) from the WBcel235 annotation using featureCounts v1.5.2 (Liao et al., 2014). Genes were only considered "testable" if they had at least 5 read-counts in a sample. After applying this filter for testable genes, 16,259 of the 20, 542 annotated protein-coding genes were retained. Differentially expressed genes between the different genotypes were identified using limma-voom (Law et al., 2014).

qPCR assays

Total RNA was isolated using using the RNAeasy mini kit (Qiagen 74104), according to manufacturer's instructions. Total cDNA was obtained using oligodT primers and the ImProm-II™ Reverse Transcription System (A3800) followed by quantitative PCR using SYBR green (Thermo Scientific 4385610) and Light Cycler 480 (Roche). The *cdc-42* reference gene was used as a control.

QUANTIFICATION AND STATISTICAL ANALYSIS

Neuronal phenotypes were analysed in 1-day adults using fluorescent reporter strains based on the position of cell bodies and axon trajectories. Axonal outgrowth and the position of cell bodies were scored as defective or normal in comparison with control animals. All phenotypic scoring was performed with minimum of two biological replicates, on independent days and at least eighty worms examined for each strain. Results were analysed using one-way ANOVA with Tukey's Multiple Comparison Test or t test on GraphPad Prism version 7, where applicable. Values were presented as mean ± SEM (standard error of the mean) and were considered statistically significant when p value is lower than 0.05: *$p < 0.05$, **$p < 0.01$, ***$p < 0.001$, ****$p < 0.0001$, n.s. not significant. All of the statistical details of the experiments can be found in the figure legends.